Wind and Structures, *Vol. 17, No. 5 (2013) 553-564*
DOI:http://dx.doi.org/10.12989/was.2013.17.5.553

A method for nonlinear aerostatic stability analysis of long-span suspension bridges under yaw wind

Wen-Ming Zhang*[1], Yao-Jun Ge[2] and Marc L. Levitan[3]

[1]*School of Civil Engineering, Southeast University, Nanjing, Jiangsu, 210096, China*
[2]*State Key Laboratory for Disaster Reduction in Civil Engineering, Department of Bridge Engineering, Tongji University, Shanghai 200092, China*
[3] *Department of Civil and Environmental Engineering, Louisiana State University, Baton Rouge, LA 70803,United States*

(Received September 25, 2012, Revised August 31, 2013, Accepted September 18, 2013)

Abstract. By using the nonlinear aerostatic stability theory together with the method of mean wind decomposition, a method for nonlinear aerostatic stability analysis is proposed for long-span suspension bridges under yaw wind. A corresponding program is developed considering static wind load nonlinearity and structural nonlinearity. Taking a suspension bridge with three towers and double main spans as an example, the full range aerostatic instability is analyzed under wind at different attack angles and yaw angles. The results indicate that the lowest critical wind speed of aerostatic instability is gained when the initial yaw angle is greater than 0°, which suggests that perhaps yaw wind poses a disadvantage to the aerostatic stability of a long span suspension bridge. The results also show that the main span in upstream goes into instability first, and the reason for this phenomenon is discussed.

Keywords: yaw wind; suspension bridge; aerostatic stability; nonlinearity

1. Introduction

With the rapid development of transportation, bridge span length has increased significantly in recent decades. To accommodate this increase, bridges have become lighter, more flexible and, accordingly, more susceptible to wind-induced problems. Recent results of wind tunnel tests and research indicate that aerostatic instability of long-span cable supported bridges is likely to occur (Cheng *et al*. 2002a, Hirai *et al*. 1967, Xie and Yamaguchi 1997). For long-span suspension bridges, they deform significantly under static wind action due to their great flexibility, and this deformation changes their stiffness and the resistant forces. On the other hand, the deformed shape of the stiffening deck produces an increase in the value of the three components of displacement-dependent wind loads distributed along the deck. When the increment of the resisting forces is less than that of static wind loads, aerostatic instability occurs (Simiu and Scanlan 1996). Therefore, aerostatic instability is a coupling effect of static wind loads and structural deformation. Currently, the aerostatic stability of long-span suspension bridges has been comprehensively investigated by Boonyapinyo *et al*. (1999, 2006), Cheng *et al*. (2002b, 2003a,b),

*Corresponding author, Assistant Professor, E-mail: wenmingzhang@hotmail.com

 ISSN: 1226-6116 (Print), 1598-6225 (Online)

Xiao and Cheng (2004), Zhang (2011). These studies developed finite element methods to predicate the critical wind speed of the nonlinear aerostatic instability for long-span suspension bridges.

While a long-span bridge scheme is planed and the bridge site and bridge axial direction are selected, the normal line direction of the bridge span is always determined to departure from the local leading wind direction to the extent possible. As a result, strong wind always attacks bridges with a yaw angle, which has been proved by site-measurement results of some long-span bridges (Zhu *et al.* 2002, 2007, Zhu and Xu 2005). However, wind direction is assumed to be normal to bridge axis in most previous studies of aerostatic stability, and few studies related to the aerostatic stability of bridges under yawed wind have been conducted to date. In addition, only the contribution from torsional deformation of the bridge deck to the change of static wind load is considered in previous studies of aerostatic stability, but the contribution from lateral deformation is not considered.

In this paper, using the nonlinear aerostatic stability theory together with the method of mean wind decomposition (Kimura and Ohara 1999, Kimura and Tanaka 1992, Scanlan 1993), a method for nonlinear aerostatic stability analysis is proposed for long-span suspension bridges under yaw wind. The contribution from the torsional deformation and that from the lateral deformation of the bridge deck to the change of static wind load are both considered in this method, which is more reasonable and accurate than previous methods. Based on this method, a computer program is developed taking into account the static wind load nonlinearity and structural nonlinearity. As a case study, full range aerostatic instability of a suspension bridge with three towers and double main spans is analyzed under wind at different attack angles and yaw angles. The relationship between critical wind velocity and yaw angle is studied. The aerostatic instability configuration of the suspension bridge is also discussed.

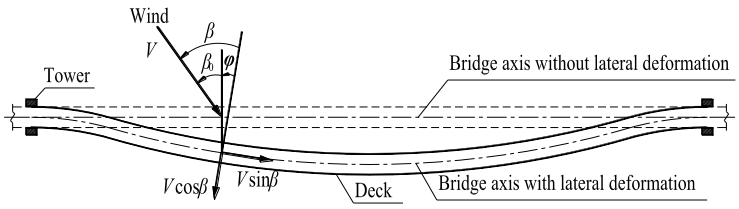

Fig. 1 Yaw angle of wind in a bridge plan

2. Proposed method

2.1 Definition of yaw angle

As shown in Fig.1, the initial yaw angle β_0 is defined as the angle between the mean wind and the bridge axis without lateral deformation in horizontal plane. While the lateral deformation occurs as an effect of wind load, any point on the bridge deck has a lateral bending angle φ, i.e., the angle between the normal line of the bridge axis in the reference configuration and that of the

bridge axis with lateral deformation. The effective yaw angle β is defined as the angle between the mean wind and the bridge axis with lateral deformation in horizontal plane, thus $\beta=\beta_0+\varphi$. It is interesting to note that the value of β or φ varies with the location on the bridge deck.

Using the method of mean wind decomposition, the mean wind velocity V is decomposed into the cosine component $V\cos\beta$ and the sinusoidal component $V\sin\beta$ in horizontal plane, which are normal to and parallel with the bridge axis with lateral deformation, respectively, as shown in Fig. 1.

2.2 Definition of attack angle

As shown in Fig. 2, the initial attack angle α_0 is defined as the angle between the cosine component $V\cos\beta$ and the bridge deck without torsional deformation. While torsional deformation occurs as an effect of wind load, any point on the bridge deck has a torsional displacement θ. The effective attack angle α is defined as the angle between the cosine component $V\cos\beta$ and bridge deck with torsional deformation, thus $\alpha=\alpha_0+\theta$.

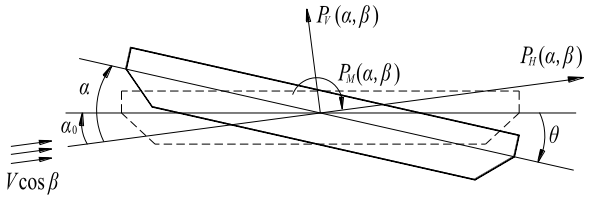

Fig. 2 Attack angle of wind and three components of wind load

2.3 Decomposition of wind load

As also shown in Fig. 2, the three components of wind load per unit span that the cosine component $V\cos\beta$ applies to the bridge deck are drag force, lift force and pitch moment, which are all functions of the effective attack angle α and the effective yaw angle β and are expressed as

$$\begin{aligned} P_H(\alpha,\beta) &= \rho(V\cos\beta)^2 C_H(\alpha)h/2 \\ P_V(\alpha,\beta) &= \rho(V\cos\beta)^2 C_V(\alpha)b/2 \\ P_M(\alpha,\beta) &= \rho(V\cos\beta)^2 C_M(\alpha)b^2/2 \end{aligned} \tag{1}$$

where P_H, P_V and P_M are drag force, lift force and pitch moment, respectively; ρ is the air density; $C_H(\alpha)$, $C_V(\alpha)$ and $C_M(\alpha)$ are the coefficients of drag force, lift force, and pitch moment in wind axes, respectively; b is the deck width; and h is the vertical projected area of the deck.

The angle between the sinusoidal component $V\sin\beta$ and the bridge deck is $\gamma=\arctan(\tan\alpha_0/\tan\beta)$ in the vertical plane through the bridge axis. In the vertical plane through the bridge axis, the sinusoidal component $V\sin\beta$ is decomposed into $V\sin\beta\cos\gamma$ and $V\sin\beta\sin\gamma$, which are parallel with and normal to the bridge axis, respectively. The value of $V\sin\beta\sin\gamma$ is so small that it can be ignored. The $V\sin\beta\cos\gamma$ applies friction force $F(\beta)$ on the surface of deck (Ministry of

Communications of the People's Republic of China 2004), which can be written as

$$F(\beta) = \rho(V\sin\beta\cos\gamma)^2 c_f s / 2 \tag{2}$$

where c_f is the friction coefficient between wind and deck surface; s is the perimeter of the deck crossing section.

When the said method is used to decompose the wind load acting on the bridge deck, only the coefficients of three component wind load are needed, which can be gained in regular aerostatic force tests of sectional model in wind tunnel. The coefficients of six component wind load (Zhu *et al*. 2002), which only can be gained using a six component scale in sectional model wind tunnel test, are not needed. This method is simple and convenient to use, and suitable for bridges with single-box deck especially.

As for the static wind loads on the towers and cables, only the drag forces along and normal to the bridge are considered.

2.4 Nonlinear iterations

The stability problem under static wind load is the combination of the nonlinear behavior of static wind load and the spatial stability theory, and can be solved using the updated Lagrange incremental method. Corresponding U.L. incremental expression can be written as

$$([K_L(\delta_{j-1})]+[K_{\sigma_{j-1}}(\delta_{j-1})]^{G+W})\bullet\{\Delta\delta_j\} = \{P_j(V_i,\alpha_j,\beta_j)\}-\{P_{j-1}(V_i,\alpha_{j-1},\beta_{j-1})\} \tag{3}$$

where $[K_L(\delta_{j-1})]$ and $[K_{\sigma_{j-1}}(\delta_{j-1})]^{G+W}$ are, respectively, the structural elastic stiffness matrix and the geometrical stiffness matrix, which are computed using the displacements δ and stresses σ from the preceding iterations; superscripts G and W refer to the gravity and wind loads, respectively; $\{\Delta\delta_j\}$ is the incremental displacement vector; $\{P_j(V_i, \alpha_j, \beta_j)\}$ is the displacement-dependent wind load vector computed using the current effective attack angles and yaw angles of wind; and $\{P_{j-1}(V_i, \alpha_{j-1}, \beta_{j-1})\}$ is the displacement-dependent wind load vector computed using the preceding effective attack angles and yaw angles of wind.

Structural stiffness and static wind loads are functions of structural displacement; therefore, the iterative method must be used when Eq. (3) is solved. The procedure of calculating critical velocity by this method can be summarized as follows:

1. Assume an initial wind velocity V_0, a wind velocity increment ΔV, and prescribed tolerance of wind velocity increment ΔV_{tol}; present wind velocity $V = V_0$.
2. Calculate wind load of the structure at V.
3. Solve the global equilibrium Eq. (3) for displacement $\{\delta\}$ by Newton–Raphson method.
4. Determine the torsional angle of element from the displacement $\{\delta\}$ by averaging the torsional displacement between left node and right node, then calculate the effective attack angle α of wind; determine the lateral bending angle of element from the displacement $\{\delta\}$ by dividing the difference of lateral displacement between left node and right node by the element length, then calculate the effective yaw angle β of wind.
5. Check if both the Euclidean norms of the effective attack angle and effective yaw angle are less than the prescribed tolerance. The Euclidean norms are written as

$$\left\{\frac{\sum_{i=1}^{N_a}(\alpha_j-\alpha_{j-1})^2}{\sum_{i=1}^{N_a}\alpha_{j-1}^{\ 2}}\right\}^{1/2} \le \varepsilon_k \tag{4a}$$

$$\left\{\frac{\sum_{i=1}^{N_a}(\beta_j-\beta_{j-1})^2}{\sum_{i=1}^{N_a}\beta_{j-1}^{\ 2}}\right\}^{1/2} \le \varepsilon_k \tag{4b}$$

where N_a is the number of nodes subjected to the displacement-dependent wind load; i is the serial number of current iteration; α and β are, respectively, the effective attack angle and effective yaw angle; and ε_k is the prescribed tolerance.

If satisfied, then add wind velocity according to scheduled change in wind velocity length, $V=V+\Delta V$. Otherwise repeat steps (2)–(5) until both Eqs. (4(a)) and (4(b)) are satisfied.

6. If the iterations do not converge at a certain velocity, then revisit previous wind velocity and recalculate by shortening the wind velocity increment, $\Delta V=\Delta V/2$, until the difference between two successive wind velocities is less than the prescribed tolerance.

Base on this method, a corresponding program is developed, and the flow chart of the program is shown in Fig. 3.

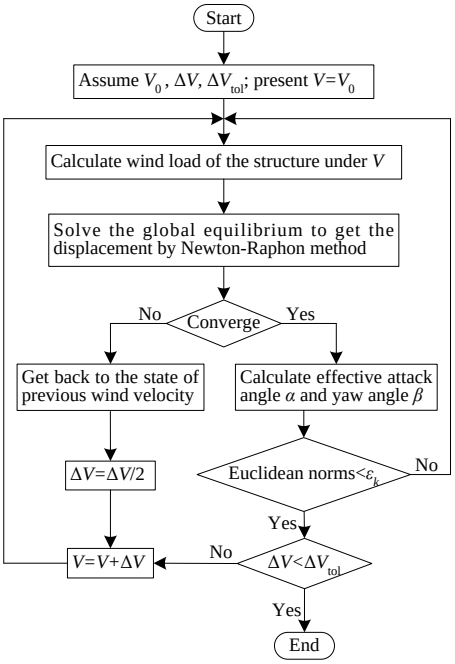

Fig. 3 Flow chart of the program

3. Description of an engineering example

The Maanshan suspension bridge over the Yangtze River in Anhui Province of China is used as an example. This bridge with double main spans is spanned as 360+2×1080+360 m in Fig. 4. All three towers are 176 m high. The height of middle tower above the deck is 128 m; the height of each side tower above the deck is 143 m symmetrically. The deck cross section is an aerodynamically shaped closed box steel deck 38.5 m wide and 3.5 m high. The two cables and all hangers are made of high tensile galvanized parallel wire bundles. The distance between the two cables is 35 m. The spacing between two adjacent hangers is 16.0 m. Section material and geometrical features of main members are indicated in Table 1. The deck is fixed with the middle tower. There are two one-way longitudinal movable supports under the deck on the lower crossbeam of each side tower; lateral wind-resistant supports are set between the deck and the columns of side towers.

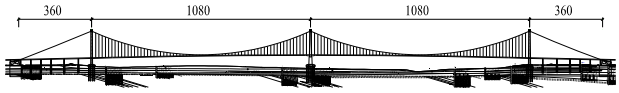

Fig. 4 Elevation of Maanshan bridge (unit: m)

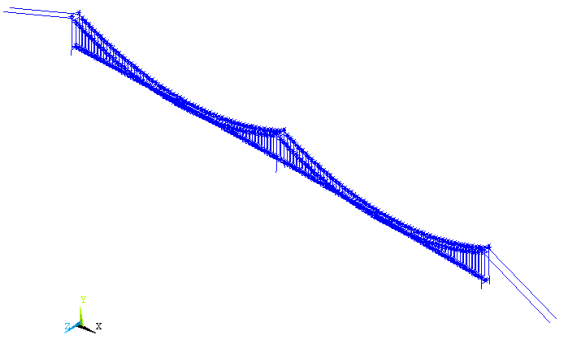

Fig. 5 Finite element model of Maanshan bridge

Table 1 Section geometrical and material features of main members

Main member	J_d (m^4)	I_2 (m^4)	I_3 (m^4)	M (t/m)	E (MPa)	v
Deck	9.10	207.04	3.22	21.39	2.01×10^5	0.3
Cable	–	–	–	2.40	2.01×10^5	–
Hanger	–	–	–	0.04	2.01×10^5	–

M: mass per unit length; E: modulus of elasticity; J_d: torsional moments of inertia; I_2: out-of-plane moments of inertia; I_3: in-plane moments of inertia; v: Poisson ratio

As shown in Fig. 5, a three-dimensional finite element model was established for the Maanshan suspension bridge. Three-dimensional beam elements are used to model the three bridge towers. The cables and suspenders are modeled by three-dimensional link elements accounting for

geometric nonlinearity due to cable sag. The bridge deck is represented by a single beam, and the cross-section properties of the bridge deck are assigned to the beam as equivalent properties. The connections between bridge components and the supports of the bridge are properly modeled. The aerostatic coefficients of the deck are obtained from the sectional model test in wind tunnel as shown in Fig. 6.

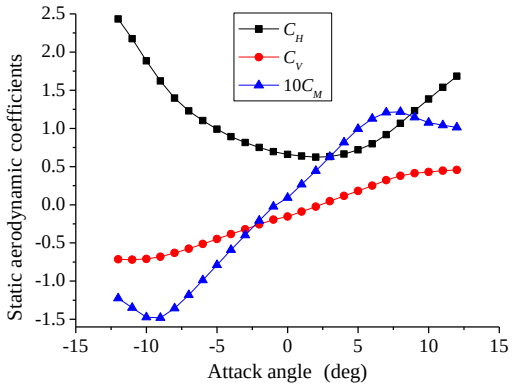

Fig. 6 Aerostatic coefficients as functions of attack angle

4. Aerostatic stability analysis

The attack angle of strong wind in atmospheric boundary layer varies within -3°~3°. In following analysis of the aerostatic stability of the Maanshan bridge, a total of five initial attack angles, -3°, -1.5°, 0°, 1.5° and 3°, and eight initial yaw angles, 0°, 3.5°, 7.5°, 15°, 22.5°, 30°, 45° and 60°, are selected. A total of 40 resultant cases are produced with different initial attack angles and initial yaw angles. Taking the bridge structure only subjected to dead load as the initial state, full-range nonlinear aerostatic stability is computed using the program presented in this paper.

4.1 Effect of initial yaw angle

The critical wind velocities under different initial attack angles and initial yaw angles are summarized in Table 2. It is to be noted that all the wind velocities in Table 2 are referenced at deck elevation. In Table 2, '>' means the critical wind velocity is greater than a certain wind velocity, at which the effective attack angle of a certain deck element is beyond the range of -12°~12° for the first time. Because aerostatic coefficients are not available beyond the attack angle range of -12°~12°, the program stops automatically at the wind velocity following the '>'. In the case of α_0=1.5° and β_0=7.5°, the lowest critical wind velocity 98.8 m/s is obtained, which is much greater than the allowable wind velocity 47.2 m/s, so the aerostatic-stability performance of the Maanshan bridge is good.

The curves of the critical wind velocity varying with the initial yaw angle are shown in Fig. 7. As can be seen, the critical wind velocity for a certain initial attack angle increases with the initial yaw angle in a general trend, and the initial yaw angle has a major effect on the critical wind velocity. However, as for the initial attack angle 0° and 1.5°, the lowest critical wind velocity that

engineers are most concerned with is not gained at β_0=0°, which suggests it is not the most dangerous case when the wind is normal to the bridge axis. This phenomenon is worthy of note.

Table 2 Critical wind velocities (m/s)

β_0 \ α_0	-3°	-1.5°	0°	1.5°	3°	Minimum
0°	>152.0	110.0	109.0	100.6	117.8	100.6
3.5°	>153.0	110.0	110.0	101.0	118.0	101.0
7.5°	>154.0	113.8	109.0	98.8	118.8	98.8
15°	>160.0	110.0	108.0	99.0	121.8	99.0
22.5°	>167.5	113.8	111.0	>120.0	126.0	111.0
30°	>176.0	119.8	116.0	>127.8	134.0	116.0
45°	156.0	151.9	144.0	>155.2	162.0	144.0
60°	212.0	211.2	200.0	>213.9	222.0	200.0

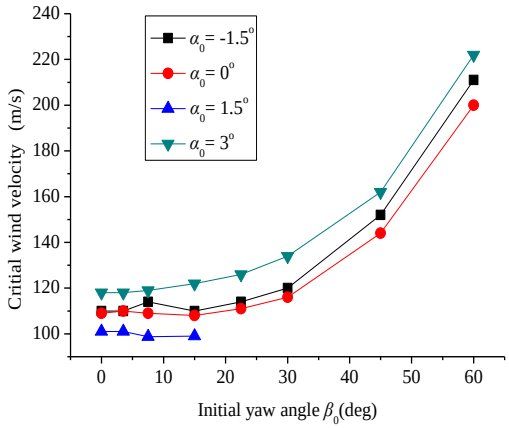

Fig. 7 Critical wind velocity varying with the initial yaw angle

4.2 Configuration of aerostatic instability

The computing result indicates that the longitudinal, vertical, lateral and torsional displacements of the deck increase nonlinearly with wind velocity. At the critical wind velocity, the displacements diverge, which means the instability of the bridge structure occurs under the static wind load and the dead load. As is known from observing the aerostatic-instability course of the bridge, the posture of the bridge changes from the initial equilibrium state as wind velocity increases, and the lateral deformation and torsional deformation cause the change of the effective yaw angle and the effective attack angle, respectively. Therefore, the static wind load acting on the bridge structure develops nonlinearly with wind velocity. Accordingly, nonlinear characteristics of various structural deformations are presented in different degrees with wind velocity. As examples, the displacement behaviors at the midpoints of both spans for the initial yaw angle 45° and initial attack angles of -3°, 0° and +3 ° are shown in Figs. 8, 9 and 10, respectively.

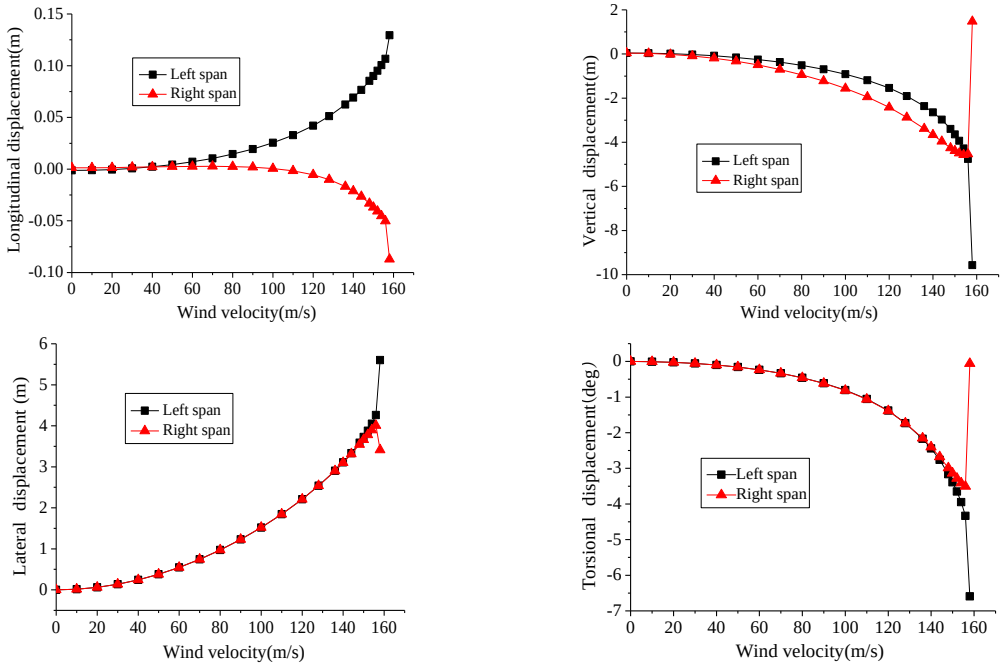

Fig. 8 The displacement behavior at the midpoints of both spans (β_0=45°, α_0= -3°)

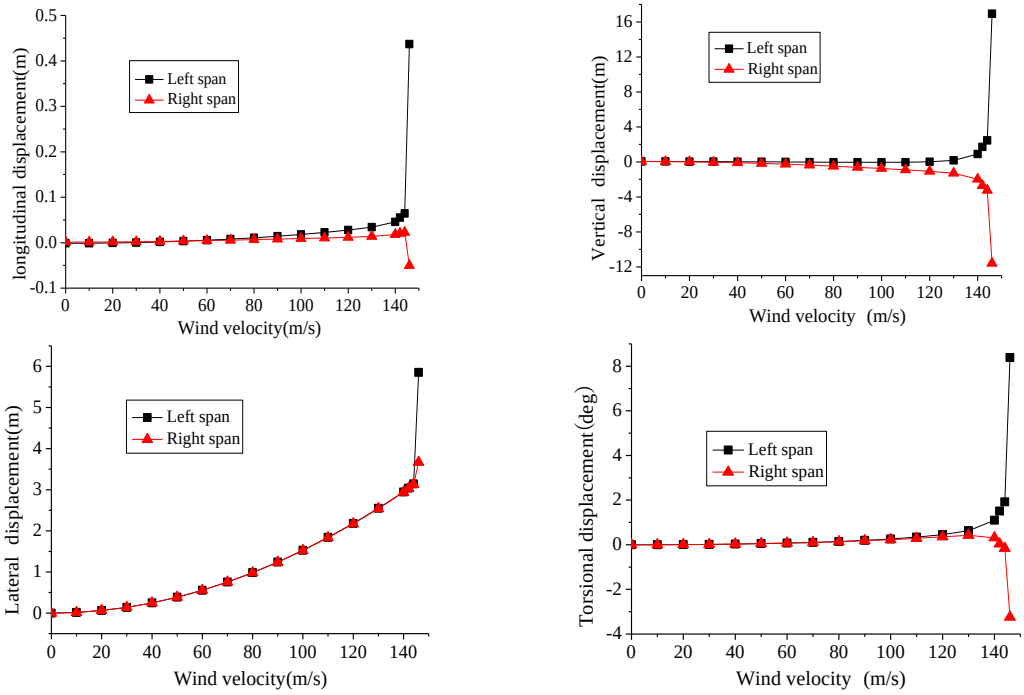

Fig. 9 The displacement behavior at the midpoints of both spans (β_0=45°, α_0=0°)

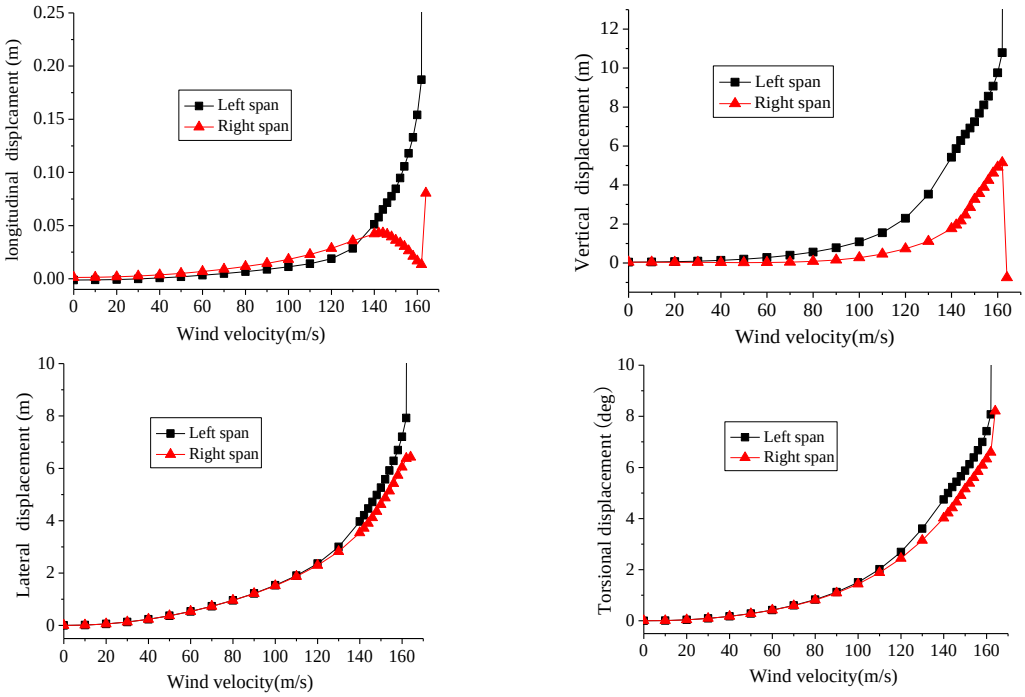

Fig. 10 The displacement behavior at the midpoints of both spans (β_0=45°, α_0=3°)

As shown in Figs. 8, 9 and 10, the displacement at the midpoint of left span is almost same as that of the right span when wind velocity is low, and the displacements at the midpoint of both spans increase nonlinearly as wind velocity increases. However, the displacement at the midpoint of the left span increases more rapidly than that of the right span when wind velocity approaches the critical wind velocity, causing the left span to go into instability first. This is because: (1) the deck is fixed with the middle tower; (2) the wind friction load along the bridge deck engenders axial pressure in the left span and axial tensile force in the right span; and (3) accordingly, the geometrical stiffness of the left span decreases, whereas that of the right span increases. The deformation of the left span is greater than that of the right span in the configuration of aerostatic instability. It is interesting to note that the left span is in the upstream of the yaw wind.

5. Conclusions

The concluding remarks about the aerostatic stability of a suspension bridge with double main spans under yaw wind and the method proposed in this paper can be summarized as follows:

1. The lowest critical wind velocity of aerostatic instability is gained when the initial yaw angle is 7.5° and the initial attack angle is 1.5°, and is much greater than the allowable wind velocity; therefore, the aerostatic-stability performance of the Maanshan Bridge is good.
2. Since the lowest critical wind speed of aerostatic instability is gained when the initial yaw angle is greater than 0°, yaw wind may pose a disadvantage to the aerostatic stability of a long span suspension bridge. The effect of the yaw angle of wind should be taken into account when

the aerostatic stability of a long-span suspension bridge is analyzed.

3. The yaw angle of wind has a major effect on the critical wind velocity of aerostatic instability.

4. The displacement behaviors of two spans under the displacement-dependent wind loads exhibit strong nonlinearity in different degrees.

5. The upstream span goes into instability first, mainly because of the wind friction load along the bridge deck.

6. Based on the nonlinear aerostatic stability theory together with the method of mean wind decomposition, the method for analyzing the nonlinear aerostatic stability of long-span suspension bridges under yaw wind is practical, simple, and convenient to use.

Acknowledgements

The work described in this paper was financially supported by the NSFC under the Grant 51208104, a project supported by the Natural Science Foundation of Jiangsu Province (Grant No. BK2012344), the RFDP under the Grant 20120092120018, and a project funded by the Priority Academic Program Development of Jiangsu Higher Education Institutions (PAPD), which are gratefully acknowledged. The writers also want to thank Ms. Kim Wyble for improving the English of this paper.

References

Boonyapinyo, V., Lauhatanon, Y. and Lukkunaprasit, P. (2006), "Nonlinear aerostatic stability analysis of suspension bridges", *Eng. Struct*., **28**(5), 793-803.

Boonyapinyo, V., Miyata, T. and Yamada, H. (1999), "Advanced aerodynamic analysis of suspension bridges by state-space approach", *J. Struct. Eng. - ASCE*, **125**(12), 1357-1366.

Cheng, J., Jiang, J.J., Xiao, R.C. and Xiang, H.F. (2002a), "Advanced aerostatic stability analysis of cable-stayed bridges using finite-element method", *Comput. Struct*., **80**(13), 1145-1158.

Cheng J., Jiang J.J., Xiao R.C. and Xiang H.F. (2002b), "Nonlinear aerostatic stability analysis of Jiang Yin suspension bridge", *Eng. Struct*., **24**(6), 773-781.

Cheng, J., Jiang, J.J. and Xiao, R.C. (2003a), "Aerostatic stability analysis of suspension bridges under parametric uncertainty". *Eng. Struct*., **25**(13), 1675-1684.

Cheng, J., Xiao, R.C, Xiang, H.F. and Jiang, J.J. (2003b), "NASAB: a finite element software for the nonlinear aerostatic stability analysis of cable-supported bridges", *Adv. Eng. Softw*., **34**(5), 287-296.

Hirai, A, Okauchi, I, Ito, M and Miyata, T. (1967), "Studies on the critical wind velocity for suspension bridges", *Proceedings of the International Research Seminar on Wind Effects on Buildings and Structures*. Ontario: University of Toronto Press.

Kimura, K. and Ohara, T. (1999), "Lateral sway buffeting of bridge decks due to yawed wind", *Proceedings of the 10th International Conference on Wind Engineering: Wind Engineering into 21st Century, Copenhagen*, Denmark. June.

Kimura, K. and Tanaka, H. (1992), "Bridge buffeting due to wind with yaw angles", *J. Wind Eng. Ind. Aerod*., **42**(1-3), 309-1320.

Ministry of Communications of the People's Republic of China. (2004), *Wind-Resistant Design Specification for Highway Bridge*, Beijing: China Communications Press (in Chinese).

Scanlan, R.H. (1993), "Bridge buffeting by skew winds in erection stages", *J. Eng. Mech. - ASCE*, **119**(2), 251-269.

Simiu, E and Scanlan, R.H. (1996), *Wind effects on structures: fundamentals and applications to design*, 3rd

Ed., New York, John Wiley and Sons.
Xiao, R.C. and Cheng, J. (2004), "Advanced aerostatic stability analysis of suspension bridges", *Wind Struct*., **7**(1), 55-70.
Xie, X. and Yamaguchi, H. (1997), "Static behaviors of self-anchored and partially earth-anchored long-span cable-stayed bridges", *Struct. Eng. Mech.*, **5**(6), 767-774.
Zhang, X.J.(2011), "Investigation on the wind-induced instability of long-span suspension bridges with 3D cable system", *Wind Struct*., **14**(3), 209-220.
Zhu, L.D., Wang, M., Wang, D.L., Guo, Z.S. and Cao ,F.C. (2007), "Flutter and buffeting performances of Third Nanjing Bridge over Yangtze River under yaw wind via aeroelastic model test", *J. Wind Eng. Ind. Aerod*., **95**(9-11), 1579-1606.
Zhu, L.D., Xu, Y.L., Zhang, F. and Xiang, H.F. (2002), "Tsing Ma bridge deck under skew winds-Part I: aerodynamic coefficients", *J. Wind Eng. Ind. Aerod*., **90**(7), 781-805.
Zhu, L.D. and Xu, Y.L. (2005), "Buffeting response of long-span cable-supported bridges under skew winds. Part 1: theory", *J. Sound Vib*., **281**(3-5), 647-673.

CC